

Fabrication of Al-TiAl₃ Composite *Via In-Situ* Accumulative Roll Bonding (ARB) and Annealing



MARYAM SAFIRI, MAHMOOD MERATIAN, and MASOUD PANJEPOUR

In this study, titanium particles (with an average size of 48 μm) are dispersed throughout Al foils using the accumulative roll bonding method. The reaction between the particles and the matrix is subsequently activated thermally by post-rolling annealing. The *in-situ* reaction between the titanium powder and the aluminum matrix promoted by mechanical activation due to accumulative roll bonding and thermal activation due to annealing leads to the formation of Ti-Al intermetallic compounds. The distribution of particles and the intermetallic compounds thus formed are characterized using X-ray diffraction (XRD), scanning electron microscopy (SEM), field-emission SEM (FESEM), electron probe micro-analysis (EPMA), and optical microscopy. The composite produced with 5 wt pct particles after 20 cycles of rolling and annealing yields the best particle distribution and TiAl₃ formation such that the only intermetallic compound formed is TiAl₃. The highest TiAl₃ contents are recorded in the Al-TiAl₃ composite formed by 20 cycles of rolling and annealed after rolling cycle numbers 5 and 9 (2 hours at 430 °C), as well as 12, 17, and 20 (2 hours at 600 °C). Surface energy is found to decrease when the most faceted particles become spherical in shape at high temperatures during the annealing process. Particles as small as 250 nm in size are also observed to form in this composite, and thus fabricated.

<https://doi.org/10.1007/s11661-018-4986-4>

© The Minerals, Metals & Materials Society and ASM International 2018

I. INTRODUCTION

COMPOSITES exhibit a good combination of physical and mechanical properties such as high thermal and electrical conductivity, good wear resistance, as well as satisfactory fatigue and fracture behavior. Moreover, metal matrix composites (MMCs) offer high strength and hardness, excellent wear resistance, and low coefficient of thermal expansion (CTE).^[1] Particle-reinforced composites have also attracted a lot of attention for their high specific moduli, high strength, good wear resistance, cost-effectiveness, and isotropic properties, among others.^[2-4] Aluminide intermetallic compounds have been satisfactorily used as reinforcements in aluminum matrix composites.^[5] Among the different kinds of aluminides, titanium aluminides are of great interest due to their high oxidation resistance and good mechanical properties at high temperatures.^[6] One of the most attractive titanium aluminides is TiAl₃ owing to its low density (3.4 g/cm³), high melting point (1350 °C), high Young's modulus (220 GPa), and

appropriate mechanical properties at both room and high temperatures.^[7,8]

The matrix-reinforcement interface plays an important role in the properties of MMCs. As loads are transferred from the matrix to the reinforcement through the interface, a strong interfacial bond is required between the two to achieve high performance of MMCs.^[9,10]

Casting, as a liquid fabrication process of MMCs, offers advantages such as low preparation cost. Its application is, however, limited by the low wettability of particles with the matrix and, thereby, the non-uniform particulate distribution.^[11] Solid-state processes are often found superior to liquid methods because such processes not only give rise to a relatively uniform particle distribution but are also capable of controlling chemical reactions at the particle-matrix interface.^[12]

From a different viewpoint, MMC fabrication processes are classified into *in-situ* and *ex-situ* ones. In the *ex-situ* methods, particles are produced independently before being introduced into the matrix.^[13] In the *in-situ* methods, however, particles are fabricated through the chemical reactions between the composite components to yield reinforcements with clean interfaces of high strength.^[14]

Accumulative roll bonding (ARB) with subsequent annealing has been used for the fabrication of metal-intermetallic composites.^[15] ARB is an appropriate method

MARYAM SAFIRI, MAHMOOD MERATIAN, and MASOUD PANJEPOUR are with the Department of Materials Engineering, Isfahan University of Technology, Isfahan 84156-83111, Iran. Contact e-mail: panjepour@cc.iut.ac.ir

Manuscript submitted February 26, 2018.

Article published online November 8, 2018

of severe plastic deformation (SPD) for MMC fabrication with advantages such as simplicity, low-cost raw materials, and high production rates. Moreover, the strong mechanical bond between the matrix and the reinforcement yields ARB products of high strength.^[16,17] In this process, mechanical activation is used as an intermediate step to increase the kinetic energy of the reactions in subsequent heat treatments.^[18]

In the present experimental work, Ti powders are dispersed in an Al matrix to change Ti particles into an intermetallic compound by repeated accumulative roll bonding and annealing. The ARB process not only serves to yield a uniform distribution of particles, but also creates bonds at the particle–matrix interface, which decreases the temperature of the mechanically activated reaction between Ti particles and Al matrix (to levels below the Al melting point). Post-rolling annealing then results in the thermal activation of the mechanically activated reaction between the particles and the matrix. This process not only provides clean particle surfaces, but also helps achieve a thermite reaction between Ti particles and Al. In contrast to *ex-situ* processes, this *in-situ* method entails no undesired reaction and, hence, no contamination of the final product.

II. MATERIAL AND METHODS

Two elemental aluminum foils (grade 1xxx, 1 mm thick, 5 cm wide, and 10 cm long) and angular titanium powder (99.9 pct pure, 48 μm in average size) were employed. Figure 1 shows a SEM image of the titanium powder used. The aluminum foils were annealed at 430 °C for 2 hours to increase their workability and later washed in acetone for degreasing. One side of each foil was then uniformly roughened using a stainless steel brush. Five weight percent titanium powder was used in three stages. In the first stage, the powder was dispersed between the brushed sides of two Al foils, which were then stacked on each other and their ends fastened with an aluminum wire. To prevent any oxide formation, the specimens were rolled in less than 120 seconds after

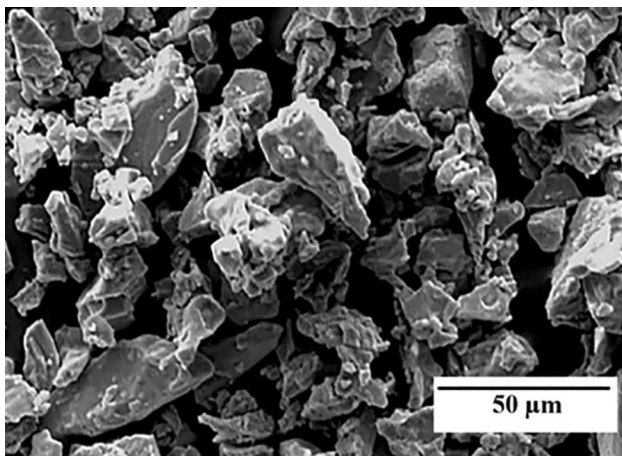


Fig. 1—SEM image of titanium powder.

surface preparation at room temperature to reach a reduction of 50 pct in all the passes. After the first cycle, the rolled strips were cut in half and each half was subjected to surface preparation.

The second and third stages of powder application were accomplished in the second and third rolling cycles, respectively. Good distribution of titanium powder was ensured by running two additional cycles. The five-cycle-rolled specimens were then annealed again at 430 °C for 2 hours in order for them to resist more strain. This was followed by four more cycles.

To investigate the effects of different numbers of rolling and annealing cycles on structural changes in the specimens, the process was repeated up to 20 cycles to obtain the different specimens reported in Table I. Annealing was performed on the specimens subjected to 5, 9, 12, and 17 cycles in order to restrict their strain capacity. It was also performed after 20 cycles to help continued Ti–Al reaction. Annealing temperature after 5 and 9 rolling cycles reached 430 °C, which was not enough for the thermal activation of the reaction. The aluminum foils were not able to resist high temperatures during their initial rolling cycles; however, they gained the capability to bear higher temperatures as titanium particle distribution improved, which led to enhanced composite strength so that the specimen subjected to 12 rolling cycles was able to be heated to 500 °C, 550 °C, and 600 °C. Thus, a temperature of 600 °C was selected for the remaining stages of the fabrication process beyond cycles 12, 17, and 20 based on the assumption that 600 °C would be the highest annealing temperature to obtain a Ti–Al intermetallic compound with no damages to the specimen.

XRD and EPMA analyses were used for the phase and elemental investigations of the specimens while their morphology and microstructural features such as particle size, distance between particles, shape factor, and intermetallic layer thickness were investigated using optical microscopy, SEM, and FESEM. The different microscopic images taken from different parts of the specimens were subjected to analysis by Image J. The Al matrix, Ti particles, and TiAl_3 were presented in three different colors. The software would use the color contrasts to measure the fraction part of each component in the composite. Moreover, the Image J would determine the shape factor of each particle by considering the circularity of particle that can be defined the similarity degree to a perfect circle and would calculate by the equation: $4\pi \times [(\text{surface area})/(\text{perimeter})^2]$. The value for each parameter was reported as the average of all the measurements of that parameter made by the Image J software using the different images. The minimum and maximum measured values were reported as negative and positive errors (outliers), respectively.

III. RESULTS AND DISCUSSION

A. Particle Distribution

Figure 2 shows the microstructural evolution of Al-5 wt pct Ti composite during the fabrication process up to 20 cycles of rolling. It is seen that agglomeration of

Ti particles reduced and their distribution in the Al matrix improved with increasing rolling cycles. Tension was not uniformly distributed in the composites

Table I. Sequential Fabrication Procedure for the Different Specimens

Specimens	Fabrication
R ₁	5 rolling cycles
A ₁	R ₁ + 2 h annealing at 430 °C
R ₂	A ₁ + 4 cycles
A ₂	R ₂ + 2 h at 430 °C
R ₃	A ₂ + 3 cycles
A ₃	R ₃ + 2 h at 600 °C
R ₄	A ₃ + 5 cycles
A ₄	R ₄ + 2 h at 600 °C
R ₅	A ₄ + 3 cycles
A ₅	R ₅ + 2 h at 600 °C

subjected to external loads since higher tensions were observed around agglomerated particles. These particles offer the sites preferred for crack generation since high tension prevents a strain flow around them. Induction of higher strains as a result of increasing rolling cycles caused the cracks generated to grow in size, which finally led to the breaking of agglomerated particles so that a completely uniform distribution of particles was achieved in the specimens subjected to 20 cycles of rolling (Figure 2(e)).

Optical image analysis of these specimens by the Image J software yielded particle counts, average particle size, shape factor, and distance between particles. Inspection of Figures 3(a) and (b) reveals that the particle count in R₅ is about 4 times that in R₁ and that the average particle size in R₅ is half that in R₁.

Figure 3(c) illustrates variations in shape factor, which increased by about 0.24 (from 0.54 to 0.78) from

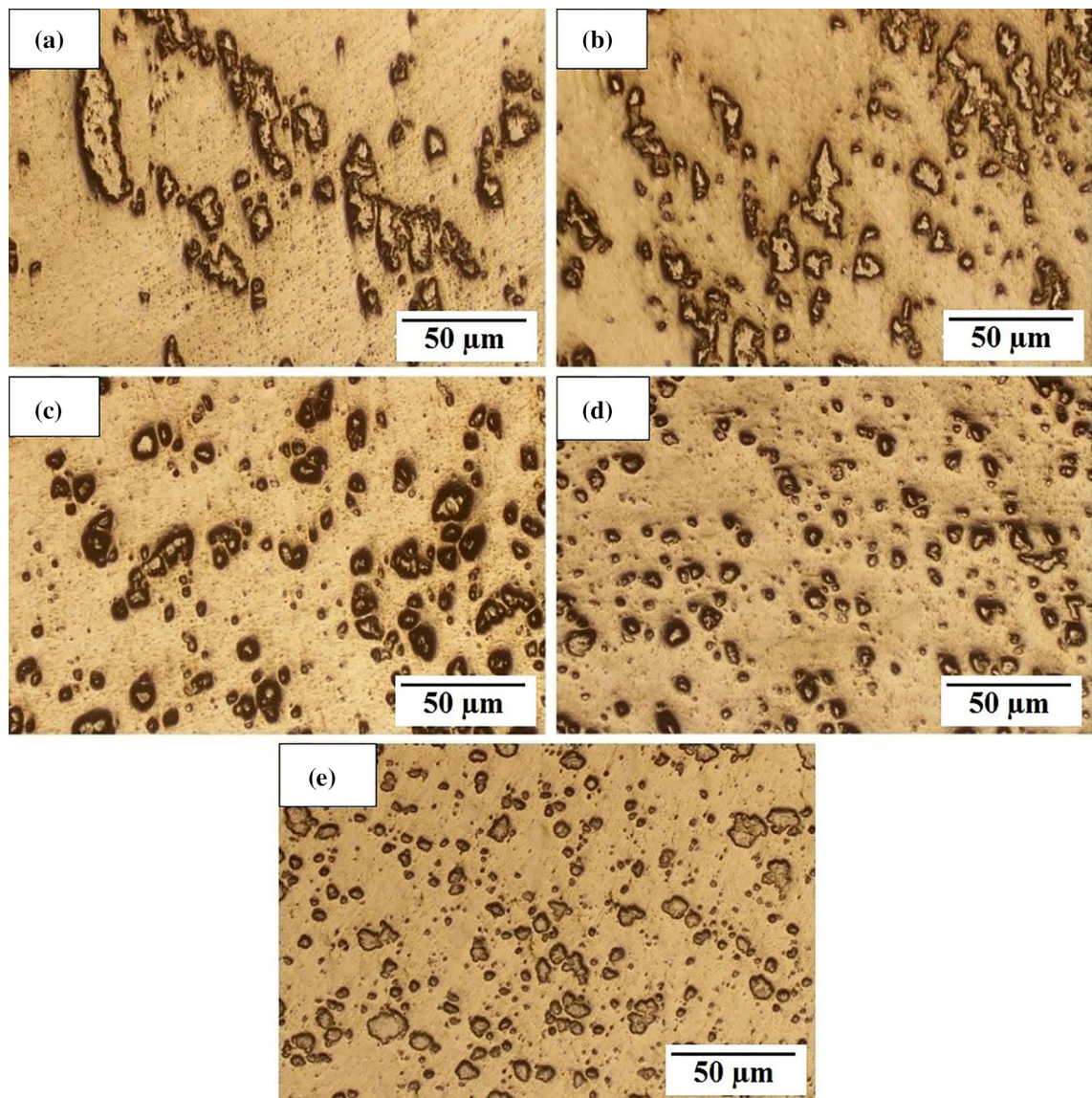


Fig. 2—Optical images of (a) R₁, (b) R₂, (c) R₃, (d) R₄, and (e) R₅ specimens.

R₁ to R₅. A higher value of shape factor represents more spherical particles created in the composite as a result of the strain applied by the ARB process. At high temperatures, particles tend to reduce in surface energy so that the particle shape approaches that of a sphere during the annealing process since spheres have the smallest surface-to-volume ratio. Moreover, the strain applied by ARB causes high aspect ratio particles to break down into spherical ones.

Figure 3(d) illustrates the distance between particles in different specimens. Clearly, this distance decreases from 17 μm in R₁ to 6 in R₅. The strain increases in aggregates as a result of more rolling cycles applied to the specimens, which then causes the particles to crush and break into more particles. The more particles there are, the smaller is the distance between them. The reduced distance between the particles then makes it more difficult for the strain to flow between particles. Finally, the harder the strain flow, the more particles are broken.

B. Phase Analysis

The ARB process not only leads to a uniform distribution of particles but also creates a mechanical bonding at the particle–matrix interface. This mechanical work during the initial stages of rolling brings Ti and Al atoms at the interface closer to each other to form intermetallic compounds. Thermal activation is then needed to give rise to the chemical reaction of Al and Ti atoms at the interface to form Ti aluminide. The required energy is generated by the post-rolling annealing process.

The XRD patterns of the specimens showed no intermetallic compounds formed as a result of the repeated rolling-annealing process up to specimen R₃. Figures 4(a), (b), and (c) present the XRD patterns of R₃ annealed at the three different temperatures of 500 °C, 550 °C, and 600 °C, respectively. As shown, annealing at 500 °C and 550 °C resulted in the formation of no intermetallic compounds. However, some peaks of TiAl₃ appeared in the XRD pattern of R₃

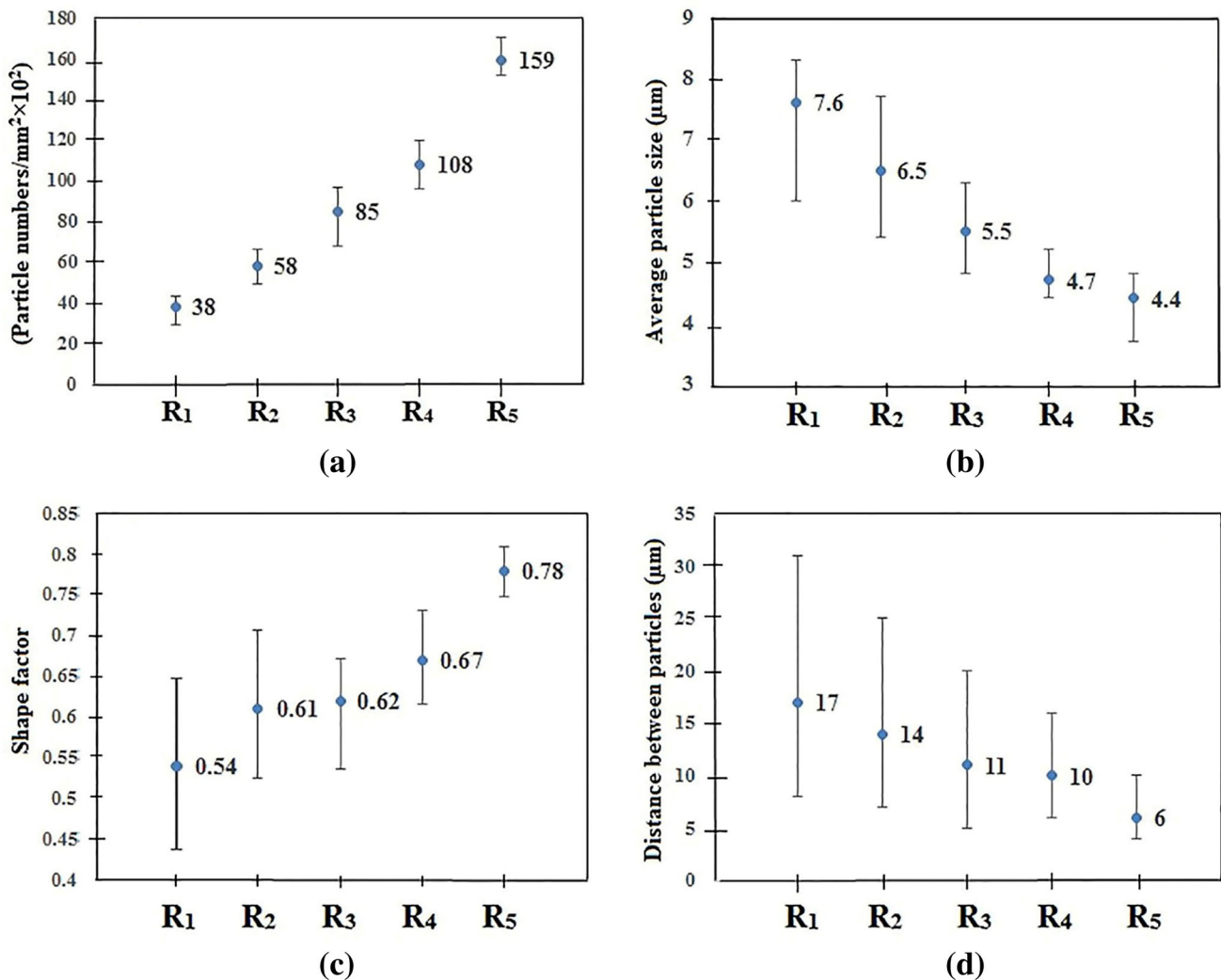


Fig. 3—(a) Particle counts, (b) average particle size, (c) shape factor, and (d) average distance between particles in different specimens.

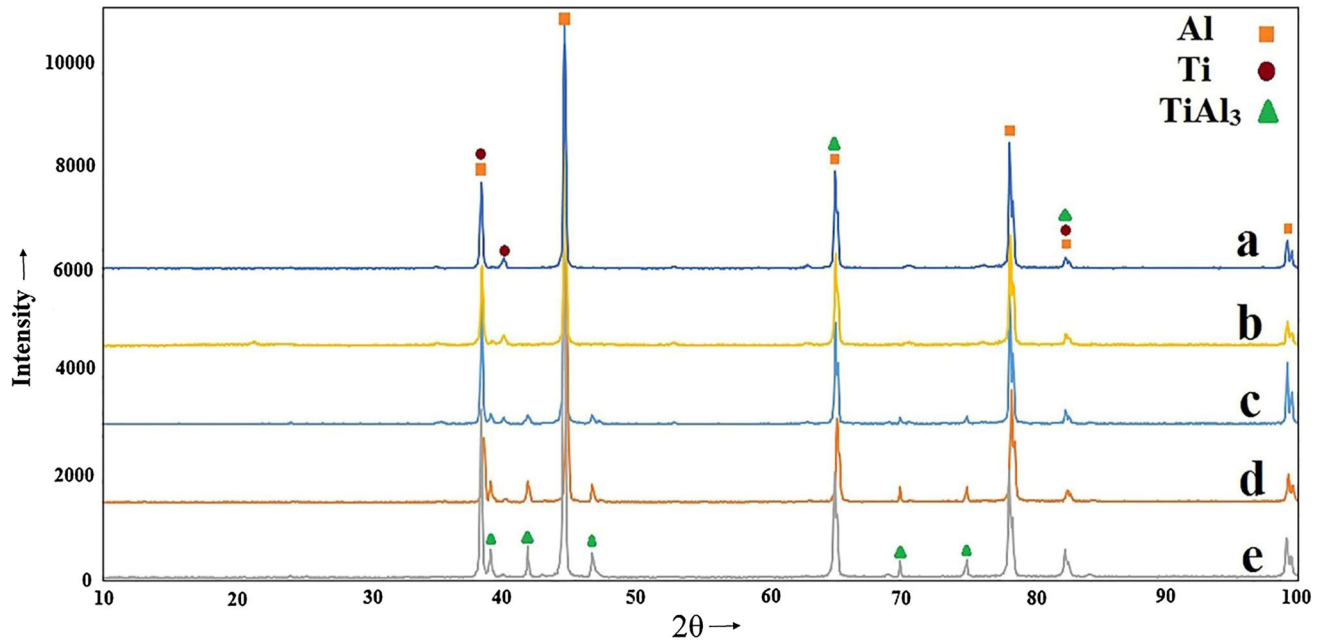
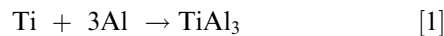


Fig. 4—XRD patterns of R₃ specimen annealed at (a) 500, (b) 550, and (c) 600 °C (A₃) as well as specimens (d) A₄ and (e) A₅.

annealed at 600 °C (A₃). Orru *et al.*^[19] reported a reaction temperature of 1244 °C. The authors predicted that the activation energy for both diffusion and intermetallic formation reactions might be reduced by mechanical activation, thereby leading to a lower reaction temperature. Chaudhari *et al.*^[20] studied Ti aluminide formation during the post-rolling annealing of Ti and Al foils. They suggested three reasons for accelerated diffusion due to ARB: (1) The refined structure and increased grain boundaries due to the strain applied to aluminum foils, (2) Increased density of lattice defects (*e.g.*, vacancies and dislocations) due to enhanced strain, and (3) Solid-state dissolution of Al and Ti due to their interdiffusion. In this study, increased diffusion as a result of the ARB process reduced this temperature to 600 °C. In addition, the rate of diffusion increased as a result of the fine particles created by the ARB process since, when diffusing through small rather than large particles, Al atoms need to pass a shorter distance to reach Ti ones, and conversely; hence, the high reaction rate of Al and Ti to create intermetallic compounds. In fact, the rate of diffusion between Al and Ti particles increased when the distance between them decreased and the interface area increased.



The XRD patterns in Figure 4 reveal that TiAl₃ was the first and only Ti aluminide formed in this process. Yang *et al.*^[21] also reported TiAl₃ as the first compound formed during the rolling-annealing process of Ti and Al foils at temperatures below Al melting point. Studying the reactions in a Ti-Al system, Sujata *et al.*^[22] verified both thermodynamically and kinetically the formation of Ti-Al intermetallic compounds.

Table II. Free Energy of Formation for Different Titanium Aluminides^[22]

Compound	Free Energy of Formation (ΔG_f)
Ti ₃ Al	− 29633.6 + 6.70801 T
TiAl	− 37445.1 + 16.79376 T
TiAl ₃	40349.6 + 10.36525 T
TiAl ₂	43858.4 + 11.02077 T
Ti ₂ Al ₅	− 40495.4 + 9.52964 T

Depending on reaction type, Ti aluminides may be classified into the following two groups: (1) Those (TiAl₃, TiAl, and Ti₃Al) formed *via* the reaction between Ti and Al, and (2) those requiring TiAl as a precursor to the formation of other compounds (*i.e.*, TiAl₂ or Ti₂Al₅). Table II reports the values for the free energy of formation (ΔG_f) required for different Ti aluminides.^[22] Thermodynamically, the lower ΔG_f value of TiAl₃ than those of TiAl and Ti₃Al (Table II) explains the easier formation of TiAl₃. Despite the higher free energy of TiAl₃ formation, compared to those of TiAl₂ and Ti₂Al₅, its formation is kinetically easier as TiAl forms necessarily prior to TiAl₂ and Ti₂Al₅. Another reason for the non-existence of other titanium aluminides is their faster diffusion in TiAl₃ so that they convert into TiAl₃ even if formed.

Apart from the A₃ specimen, the development of others was also carefully examined up to 20 cycles of repeated annealing. The XRD patterns of A₄ and A₅ are presented in Figures 4(d) and (e), respectively. As can be seen, the intensity of Ti peaks in these specimens decreased, or some even disappeared, in A₅ while those of TiAl₃ were intensified.

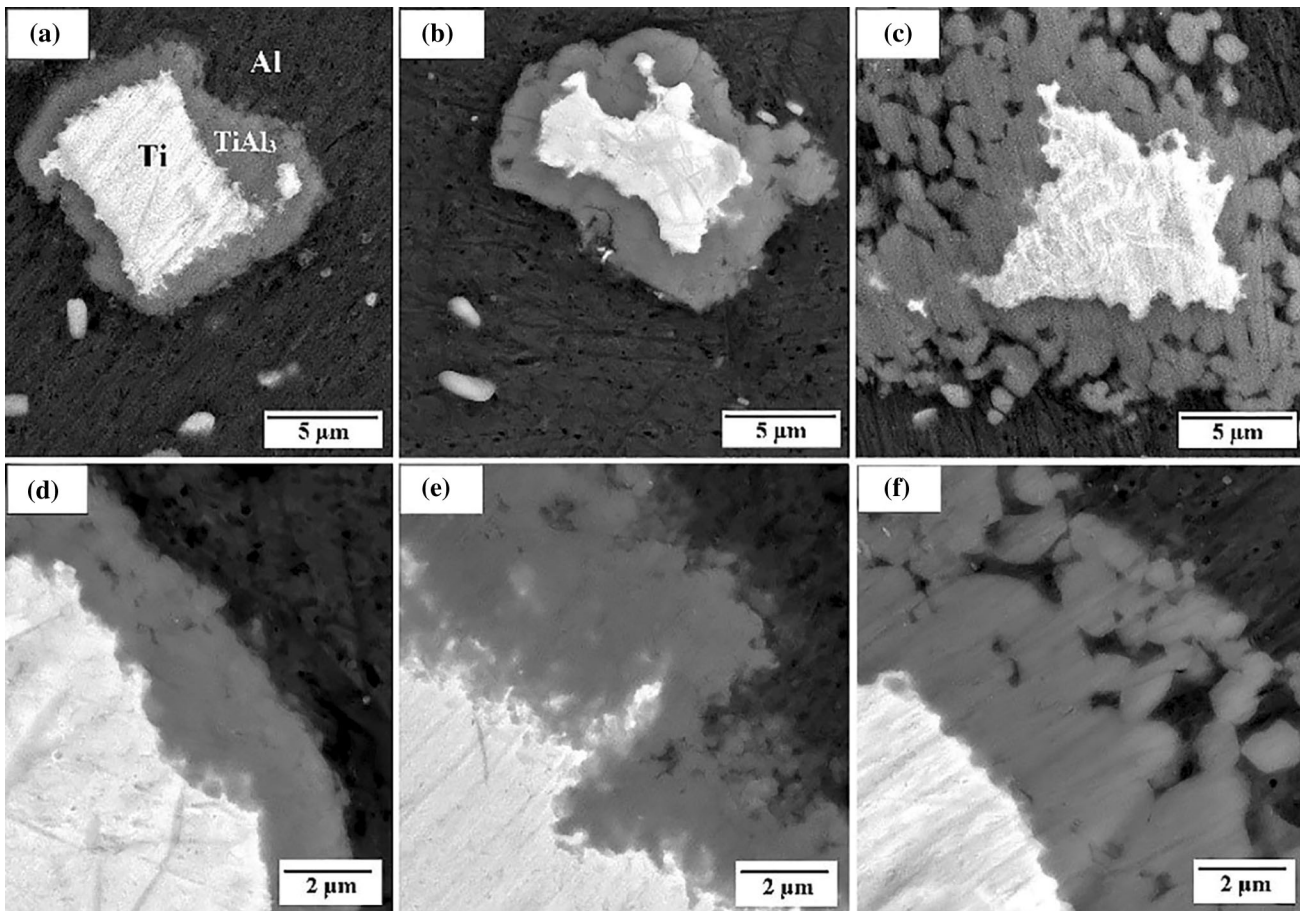


Fig. 5—FESEM images of a reacted particle in (a) A_3 , (b) A_4 , and (c) A_5 as well as the reacted layer at the interface in (d) A_3 , (e) A_4 , and (f) A_5 .

C. Microstructural Analysis

Figures 5(a), (b), and (c) present FESEM images of reacted particles in A_3 , A_4 , and A_5 , respectively, in which three different parts might be seen: a white unreacted Ti in the center of the particles, a dark aluminum matrix, and a gray reacted titanium ($TiAl_3$) at the particle–matrix interface. The reacted layers at the interface in A_3 , A_4 , and A_5 are presented in Figures 5(d), (e), and (f), respectively. Clearly, these reacted layers grow in thickness as we move from Figures 5(d) to (f) as do the percentages of particles transformed into $TiAl_3$ (as measured by the Image J software) from 51 in A_3 to 64.9 in A_4 and 74.55 pct in A_5 .

SEM images of A_3 , A_4 , and A_5 are presented at a low magnification in Figure 6. Improved particle distribution and increased $TiAl_3$ content are clearly observed in Figures 6(a) to (c). The nearly complete transformation of most of the Ti particles into $TiAl_3$ is utterly visible in Figure 6(c).

As seen in the XRD pattern of the specimen A_5 shown in Figure 4(e), most Ti peaks disappeared. In Figure 6(c), however, some small Ti peaks still remain, reflecting small amounts of Ti remaining at the center of the particles.

In their study of the formation of intermetallic compounds during the annealing of rolled Ti–Al foils, Yang *et al.*^[21] realized that $TiAl_3$ grows in two steps: (1) lateral growth parallel to the interface, and (2) thickening of this layer perpendicular to the interface. $TiAl_3$ initially creates a shell structure in the outer layer of Ti particles. Due to differences in density between $TiAl_3$ (3.13 g/cm^3) and Ti (4.46 g/cm^3),^[23] thickening of the $TiAl_3$ layer leads to differences in volume expansion, which generates tensile stresses at the center of the particles but compressive stresses at the Ti– $TiAl_3$ interface. Compressive stresses counteract the forces of rolling and make a strong bond at the Ti– $TiAl_3$ interface. On the other hand, the strain flow around the particles during the rolling process causes cracking at the outer layer of $TiAl_3$. At higher rolling cycles, these cracks grow to break the brittle $TiAl_3$ layer at the Al– $TiAl_3$ interface. Thus, parts of the $TiAl_3$ layer separated to form spherical particles (Figure 5(f)). As already mentioned, the spherical shape of the particles at this stage was due to the high energy of angular particles and their tendency to reduce this energy by reforming themselves during the annealing process as close to a spherical shape as possible.

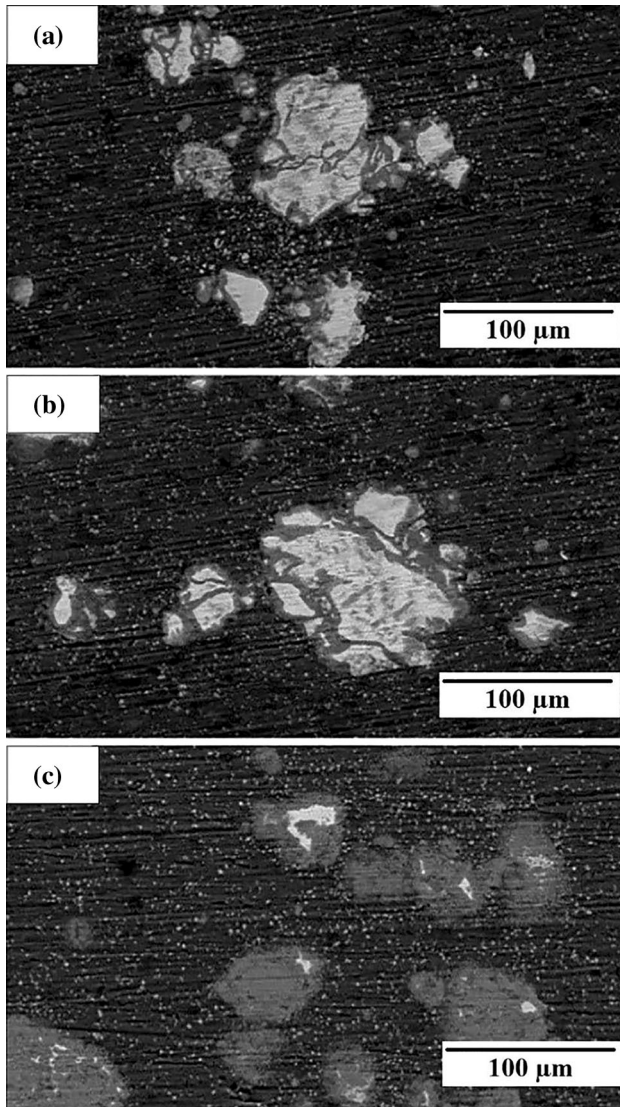


Fig. 6—SEM images of (a) A₃, (b) A₄, and (c) A₅ at low magnification.

The accumulative roll-bonded specimens lacked a uniform thickness of their reaction layer. Therefore, the average thickness of the different parts of the reaction layer was reported in Figure 7. It is seen in this Figure that the thickness of the intermetallic layer changed from 2.2 μm in A₃ to 3.5 and 4.9 μm in A₄ and A₅, respectively, with increasing cycles of rolling and annealing.

Figure 8 depicts high magnification FESEM images of small particles. Clearly, particles of the nano-scale were also created but the average size of the primary Ti powders was only 48 μm .

Rolling induces a severe plastic deformation in the composite. Thus, the mechanically activated Ti-Al reaction in rolling, as in other SPD processes such as FSP (Friction Stir Processing), takes place in two steps^[24]: (1) Coarse Ti particles are initially broken as

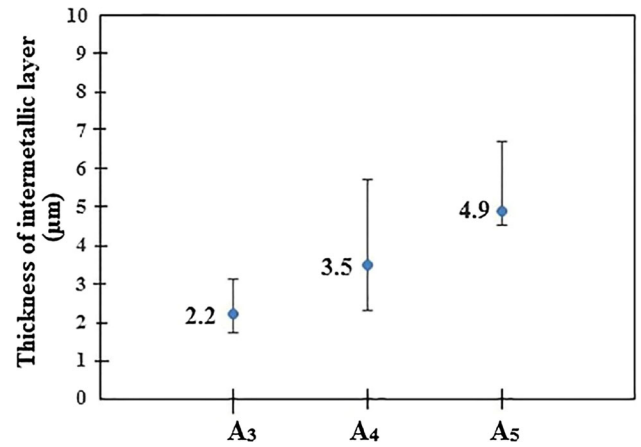


Fig. 7—Intermetallic layer thickness in A₃, A₄, and A₅.

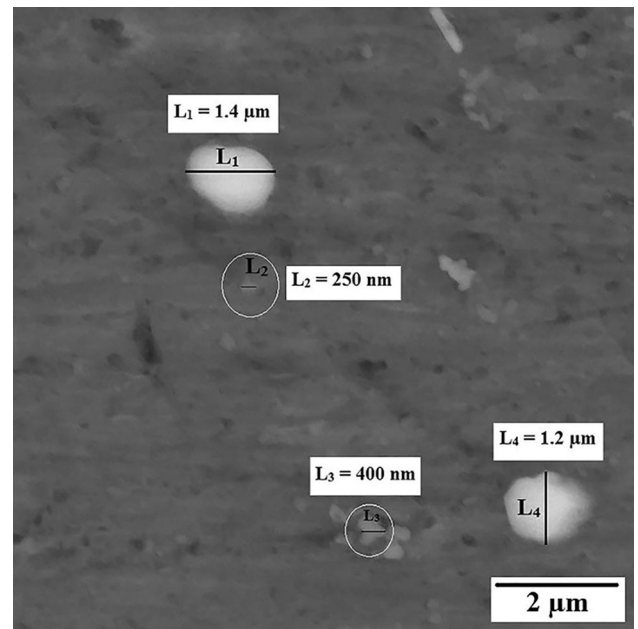


Fig. 8—FESEM images of small particles in the matrix at high magnification.

a result of severe plastic deformation and particles with clean interfaces enter into the matrix while high-density dislocations also exist in the Al matrix and Ti particles; and (2) Mechanical activation reduces the activation energy of both diffusion and interfacial particle-matrix reaction. Chemical reactions, therefore, occur at higher rates at low temperatures (reaction temperature declining from 1244 $^{\circ}\text{C}$ ^[19] to 600 $^{\circ}\text{C}$). Continued rolling cycles possibly causes TiAl₃ to separate off the interface to get distributed in the matrix in the form of fine TiAl₃ particles. As a result, not only do finer particles exist at the interface but the reduced thickness of the reaction layer also facilitates the reactions to proceed.

The formation of TiAl₃ was confirmed by both XRD patterns and EMPA analysis as reported in Figure 9. In

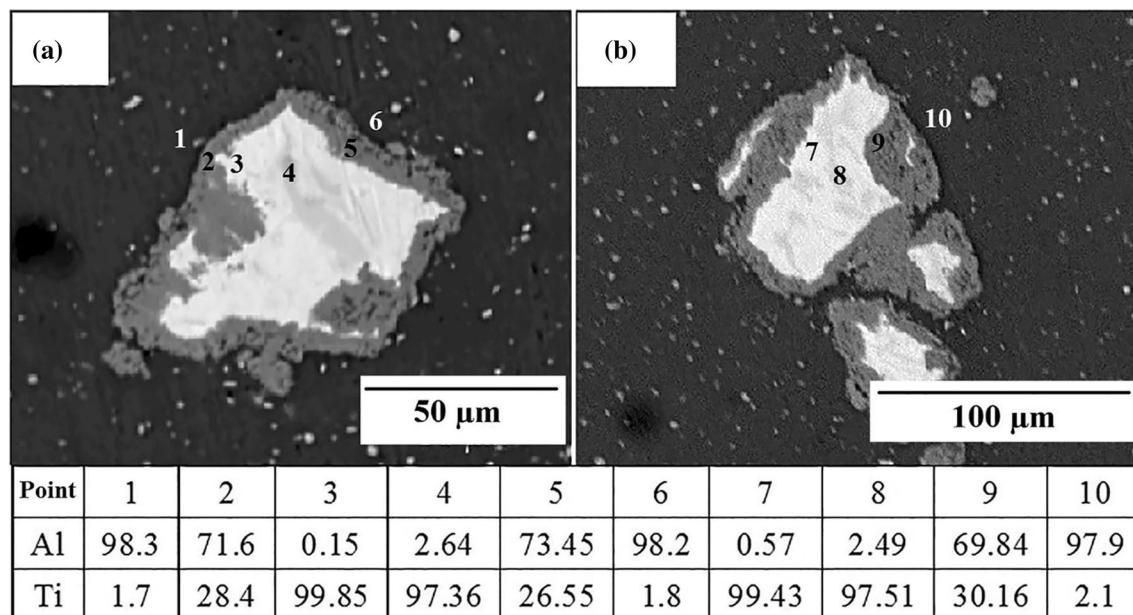


Fig. 9—EPMA analysis of different points of two different parts (*a* and *b*) in the specimen A_5 .

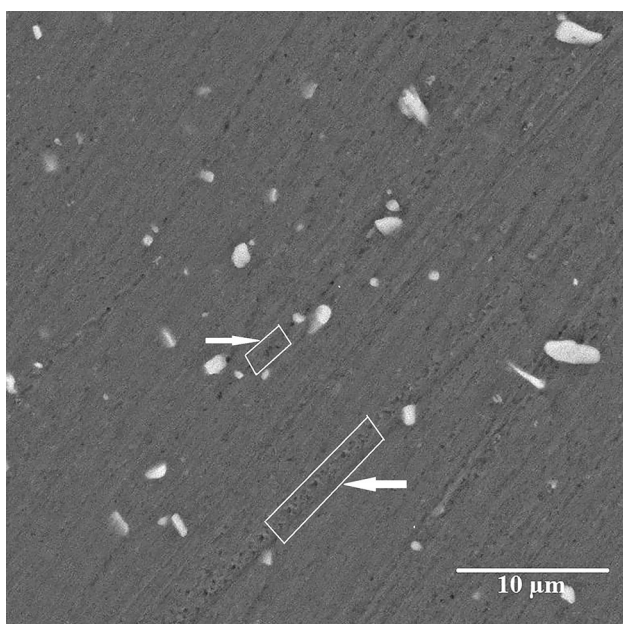


Fig. 10—Porosities observed in FESEM image of the specimen A_5 .

this Figure, points 2, 5, and 9 in the reaction layer include 71.6, 73.45, and 69.84 pct aluminum but 28.4, 26.55 and 30.16 pct titanium, respectively (representing a composition almost similar to that of the $TiAl_3$ compound).

Some porosities have been also observed in most high magnification FESEM images (Figure 10). With regard to the interdiffusion process of Al/Ti couples, Al atoms (in solid state) diffuse faster than Ti atoms at the applied temperature range, as reported in the Reference 25 For this reason, Al atoms left some porosities (known as

Kirkendall porosity) in Al matrix behind when diffusing into Ti particles.

D. Effects of Rolling-Annealing on $TiAl_3$ Formation

1. Rolling process

Figure 11 shows the effects of rolling on the progress of Al-Ti reaction. As seen in Figure 11(a), no $TiAl_3$ was formed in A_2 but that only finer particles were formed in R_3 as a result of the three additional rolling cycles performed on A_2 (Figure 11(b)). Compared to A_3 (Figure 11(c)) and A_4 (Figure 11(e)), R_4 (Figure 11(d)) and R_5 (Figure 11(f)), respectively, were only subjected to five additional rolling cycles in their fabrication process. This is while the reacted layers in R_4 and R_5 exhibited only slight increases in their thickness.

SEM images of different specimens before and after annealing are shown in Figure 12. Compared to R_3 (Figure 12(a)), R_4 (c), and R_5 (e), respectively, the specimens A_3 (Figure 12(b)), A_4 (d), and A_5 (f) each has just one additional annealing cycle in its fabrication process. Annealing, clearly, had a significant effect on the progress of the reaction such that extremely high increases are observed in the thickness of the reacted layers in A_3 , A_4 , and A_5 relative to those of R_3 , R_4 , and R_5 , respectively.

Generally speaking, the combined rolling and annealing processing of the Al-Ti composite was found not only able to transform the composite into an *in-situ* Al- $TiAl_3$ one but, also capable of yielding a highly uniform distribution of $TiAl_3$ particles, unlike in the case of Ti particles, with an average particle size of $4.4 \mu m$. Moreover, the surface energy of the particles was observed to decrease during annealing as a result of deformation into almost spherical shapes.

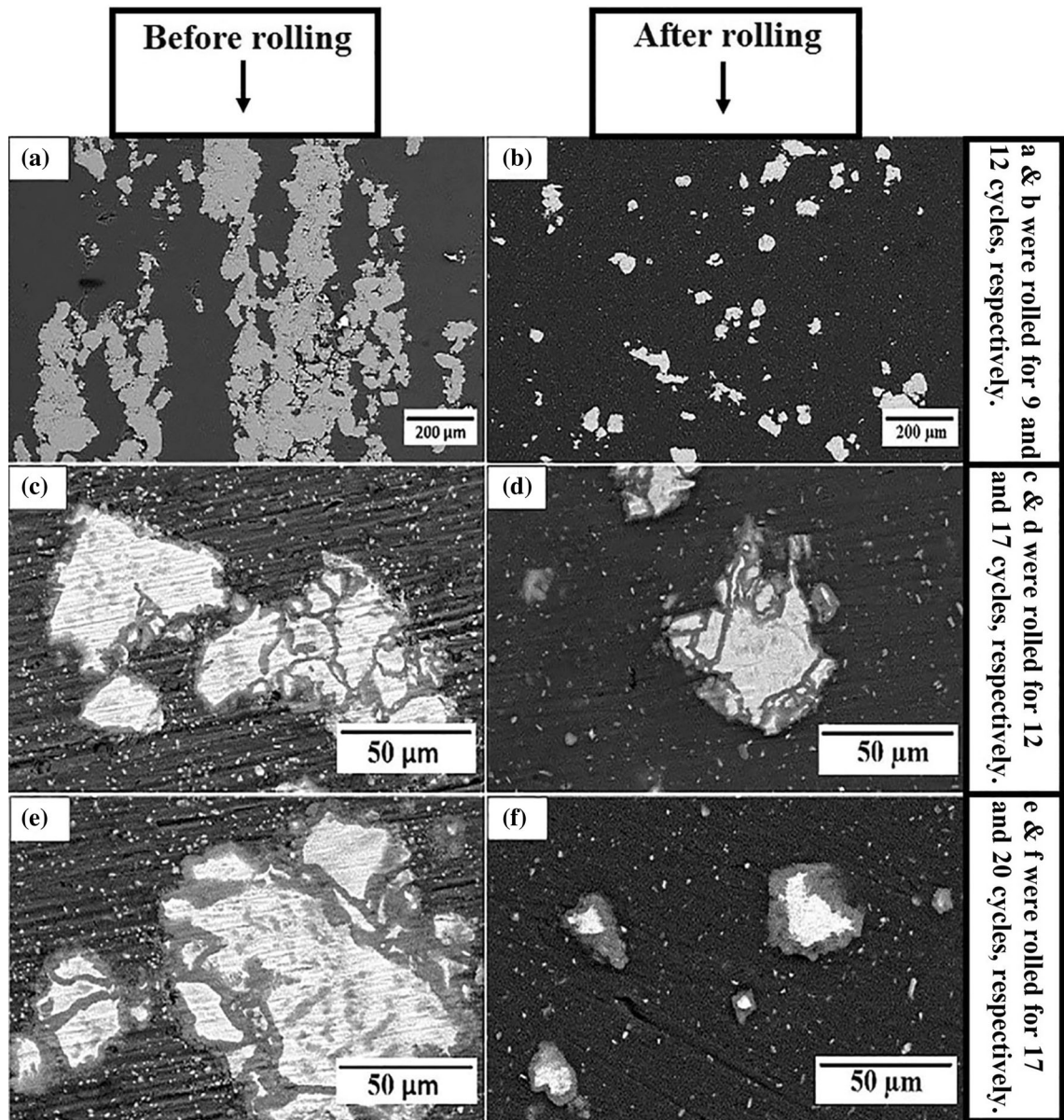


Fig. 11—SEM images of (a) A₂, (c) A₃, and (e) A₄ (before rolling) as well as (b) R₃, (d) R₄, and (f) R₅ (after rolling).

IV. CONCLUSIONS

The conclusions drawn from the findings of the present experiment may be summarized as follows:

- Increasing number of rolling cycles resulted in the uniform distribution of particles in the matrix.
- Application of strain through rolling as a mechanical process created a mechanical bonding between the particles and the matrix, which brought Al and Ti atoms at the particle–matrix interface closer to each other.
- Mechanical activation during rolling reduced the activation energy of the Al-Ti reaction so that post-rolling annealing of the specimen at 600 °C led to the formation of TiAl₃.
- Repeating rolling and annealing created an Al matrix composite with a high TiAl₃ content.
- TiAl₃ was observed to be the only intermetallic compound in this process.
- During rolling and annealing, TiAl₃ was observed to give rise to the creation of fine particles as small as 250 nm.

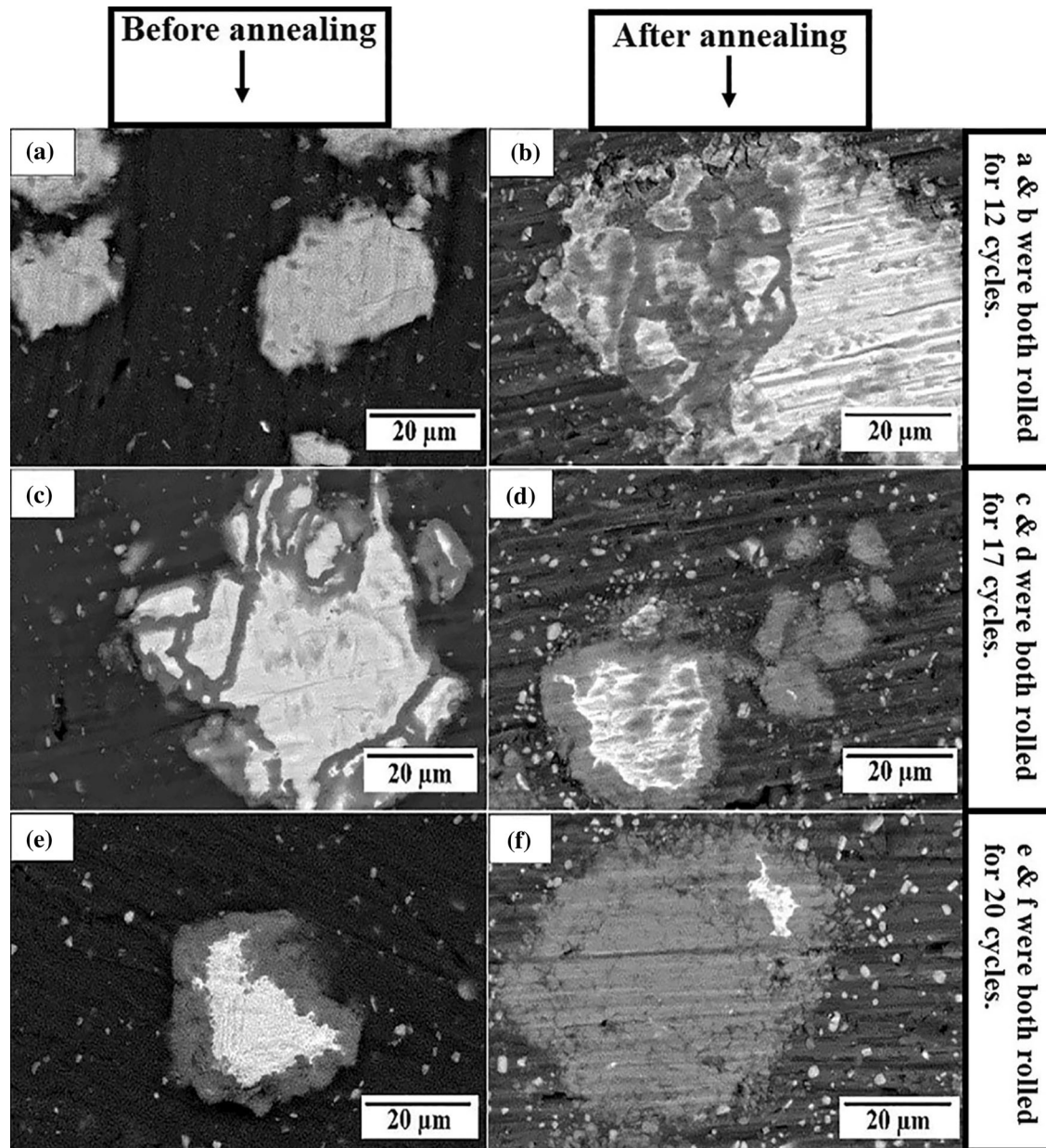


Fig. 12—SEM images of (a) R₃, (c) R₄, and (e) R₅ (before annealing) as well as (b) A₃, (d) A₄, and (f) A₅ (after annealing).

ACKNOWLEDGMENTS

The Particulate Materials Research Group at the Department of Materials Engineering, Isfahan University of Technology, deserve the authors' gratitude for their full support throughout this study. Our deep appreciation also goes to Dr. Ezzatollah Roustazadeh from ELC, IUT, for editing the final manuscript in English.

REFERENCES

1. D.B. Miracle: *Compos. Sci. Technol.*, 2005, vol. 65, pp. 2526–40.
2. N. Chawla and Y.-L. Shen: *Adv. Eng. Mater.*, 2001, vol. 3, pp. 357–70.
3. V.A. Romanova, R.R. Balokhonov, and S. Schmauder: *Acta Mater.*, 2009, vol. 57, pp. 97–107.
4. A. Yazdani and E. Salahinejad: *Mater. Des.*, 2011, vol. 32, pp. 3137–3142.
5. V. Abbasi Chianeh, H.R. Madaah Hosseini, and M. Nofar: *J. Alloys Compd.*, 2009, vol. 473, pp. 127–32.
6. S. Catchpole-Smith and A.T. Clare: *J. Mater. Process. Technol.*, 2017, vol. 239, pp. 230–39.
7. Y.U. Huashun, C. Hongmei, S. Liming, and M. Guanghui: *Rare Metals*, 2006, vol. 25, pp. 32–36.
8. Q. Zhang, B.L. Xiao, W.G. Wang, and Z.Y. Ma: *Acta Mater.*, 2012, vol. 60, pp. 7090–03.
9. X. Wang, A. Jha, and R. Brydson: *Mater. Sci. Eng. A*, 2004, vol. 364, pp. 339–45.
10. K.M. Shorowordi, T. Laoui, A. Haseeb, J.-P. Celis, and L. Froyen: *J. Mater. Process. Technol.*, 2003, vol. 142, pp. 738–43.
11. T.W. Clyne and P.J. Withers: *An Introduction to Metal Matrix Composites*, Cambridge University Press, Cambridge, 1995.
12. E. Efzan, M. Noor, N.S. Syazwani, and M.M.A.B. Abdullah: *Key Engineering Materials*, Tech Publ, Taipei, 2016, pp. 102–10.
13. S. Suresh: *Fundamentals of Metal-Matrix Composites*, Elsevier, Amsterdam, 2013.
14. Y. Afkham, R.A. Khosroshahi, S. Rahimpour, C. Aavani, D. Brabazon, and R.T. Mousavian: *Arch. Civil Mech. Eng.*, 2018, vol. 18, pp. 215–26.
15. A. Mozaffari, M. Hosseini, and H.D. Manesh: *J. Alloy. Compd.*, 2011, vol. 509, pp. 9938–45.
16. Y. Saito, N. Tsuji, H. Utsunomiya, T. Sakai, and R.G. Hong: *Scripta Mater.*, 1998, vol. 39, pp. 1221–27.
17. M. Hosseini, N. Pardis, H.D. Manesh, M. Abbasi, and D.I. Kim: *Mater. Des.*, 2017, vol. 113, pp. 128–36.
18. B.S.B. Reddy, K. Das, and S. Das: *J. Mater. Sci.*, 2007, vol. 42, pp. 9366–78.
19. R. Orru, G. Cao, and Z.A. Munir: *Metall. Mater. Trans. A*, 1999, vol. 30A, pp. 1101–08.
20. G.P. Chaudhari and V.L. Acoff: *Intermetallics*, 2010, vol. 18, pp. 472–78.
21. D. Yang, P. Hodgson, and C. Wen: *Intermetallics*, 2009, vol. 17, pp. 727–32.
22. M. Sujata, S. Bhargava, and S. Sangal: *J. Mater. Sci. Lett.*, 1997, vol. 16, pp. 1175–78.
23. A.S. Lopis, Q.G. Reynolds, and K. Bisaka: *Adv. Mater. Processes*, 2010, vol. 24, pp. 335–44.
24. Q. Zhang, B.L. Xiao, and Z.Y. Ma: *Mater. Chem. Phys.*, 2013, vol. 139, pp. 596–602.
25. L. Xu, Y.Y. Cui, Y.L. Hao, and R. Yang: *Mater. Sci. Eng. A*, 2006, vol. 435, pp. 638–47.